



1 **Airborne in-situ quantification of methane emissions**  
2 **from oil and gas production in Romania**

3 Hossein Maazallahi<sup>1,\*</sup>, Foteini Stavropoulou<sup>1,6</sup>, Samuel Jonson Sutanto<sup>1,\*\*</sup>, Michael Steiner<sup>2</sup>,  
4 Dominik Brunner<sup>2,3</sup>, Mariano Mertens<sup>4</sup>, Patrick Jöckel<sup>4</sup>, Antoon Visschedijk<sup>5</sup>, Hugo Denier  
5 van der Gon<sup>5</sup>, Stijn Dellaert<sup>5</sup>, Nataly Velandia Salinas<sup>6</sup>, Stefan Schwietzke<sup>6</sup>, Daniel Zavala  
6 Araiza<sup>6</sup>, Sorin Ghemulet<sup>7</sup>, Alexandru Pana<sup>7</sup>, Magdalena Ardelean<sup>7</sup>, Marius Corbu<sup>7</sup>, Andreea  
7 Calcan<sup>7</sup>, Stephen A. Conley<sup>8</sup>, Mackenzie L. Smith<sup>8</sup>, Thomas Röckmann<sup>1</sup>

8 <sup>1</sup> Institute for Marine and Atmospheric research Utrecht (IMAU), Utrecht University, Utrecht,  
9 the Netherlands

10 <sup>2</sup> Laboratory for Air Pollution/Environmental Technology, Empa - Swiss Federal  
11 Laboratories for Materials Science and Technology, Dübendorf, Switzerland

12 <sup>3</sup> Institute for Atmospheric and Climate Science, ETH Zurich, Zurich, Switzerland

13 <sup>4</sup> Deutsches Zentrum für Luft- und Raumfahrt, Institut für Physik der Atmosphäre,  
14 Oberpfaffenhofen, Germany

15 <sup>5</sup> Netherlands Organisation for Applied Scientific Research (TNO), Utrecht, the Netherlands

16 <sup>6</sup> Environmental Defense Fund (EDF), Berlin, Germany, and Amsterdam, the Netherlands

17 <sup>7</sup> National Institute for Aerospace Research “Elie Carafoli” (INCAS), Bucharest, Romania

18 <sup>8</sup> Scientific Aviation (SA), Inc., 3335 Airport Road Suite B, Boulder, Colorado 80301, United  
19 States

20 \* Now at: Department of Renewable Energies and Environment, College of Interdisciplinary  
21 Science and Technologies, University of Tehran, Tehran, Iran.

22 \*\* Now at: Earth Systems and Global Change, Wageningen University and Research,  
23 Wageningen, the Netherlands.

24

25 **Correspondence to:**

26 Hossein Maazallahi ([h.maazallahi@ut.ac.ir](mailto:h.maazallahi@ut.ac.ir)), Thomas Röckmann ([t.roeckmann@uu.nl](mailto:t.roeckmann@uu.nl))

27 **Abstract**

28 Production of oil and gas in Romania, one of the largest producers in the EU, is associated with  
29 substantial emissions of methane to the atmosphere and may offer high emission mitigation  
30 potential to reach the climate objectives of the EU. However, comprehensive quantification of  
31 emissions in this area has been lacking. Here we report top-down emission rate estimates  
32 derived from aircraft-based in-situ measurements that were carried out with two aircraft during  
33 the ROMEO 2019 campaign, supported by simulations with atmospheric models. Estimates  
34 from mass balance flights at individual dense production clusters, and around larger regions,  
35 show large variations between the clusters, supporting the important role of individual super  
36 emitters, and possibly variable operation practices or maintenance state across the production  
37 basin. Estimated annual total emissions from the Southern Romanian O&G infrastructure are  
38  $227 \pm 86$  kt CH<sub>4</sub> yr<sup>-1</sup>, consistent with previously published estimates from ground-based site-  
39 level measurements during the same period. The comparison of individual plumes between  
40 measurements and atmospheric model simulations was complicated by unfavorable low wind



41 conditions. Similar correlations between measured and simulated CH<sub>4</sub> enhancements during  
42 large-scale raster flights and mass balance flights suggest that the emission factor determined  
43 from a limited number of production clusters is representative for the larger regions. We  
44 conclude that ground-based and aerial emission rate estimates derived from the ROMEO  
45 campaign agree well, and the aircraft observations support the previously suggested large  
46 under-reporting of CH<sub>4</sub> emissions from the Romanian O&G industry in 2019 to UNFCCC.

## 47 1. Introduction

48 Methane (CH<sub>4</sub>) is a potent greenhouse gas with more than 80 times the global warming  
49 potential of carbon dioxide (CO<sub>2</sub>) over a 20-year time horizon (Szopa et al., 2021).  
50 Approximately 60% of global CH<sub>4</sub> emissions are attributed to human activities, with roughly  
51 one-third of them resulting from the Oil and Gas (O&G) industry (Saunio et al., 2020).  
52 Reducing CH<sub>4</sub> emissions from the O&G industry presents an easily accessible and cost-  
53 effective mitigation option (Shindell et al., 2021). Given the relatively short lifetime of CH<sub>4</sub> in  
54 the atmosphere ( $\approx 10$  years), such measures would lead to substantial climate benefits in both  
55 the near- and long-term future (Shindell et al., 2021; Collins et al., 2018). Scenarios that are  
56 compatible with the goal of the Paris Agreement (UNFCCC, 2015) to limit global warming to  
57 2 °C, preferentially to 1.5 °C all include substantial reductions in CH<sub>4</sub>, and the current growth  
58 in CH<sub>4</sub> is incompatible with reaching this goal (Nisbet et al., 2020).

59 Improving our understanding of CH<sub>4</sub> emissions from the O&G industry requires  
60 comprehensive and accurate emissions measurements using a combination of approaches.  
61 Several studies, mostly in North America, consistently show that national inventories, which  
62 rely on multiplying activity data with generic emission factors, tend to underestimate CH<sub>4</sub>  
63 emissions from the O&G industry (Allen et al., 2013; Brandt et al., 2014; Harriss et al.,  
64 2015; Johnson et al., 2017; Alvarez et al., 2018; Weller et al., 2020).

65 CH<sub>4</sub> emissions can be quantified using top-down or bottom-up approaches. Top-down  
66 approaches use ambient CH<sub>4</sub> mole fraction measurements from aircraft, tall towers, weather  
67 stations or satellites, combined with models to estimate the total CH<sub>4</sub> flux rate at different scales  
68 (i.e., site-level to regional or country-level). These approaches ensure that emissions from all  
69 sources are captured. Other techniques, such as the use of ethane (C<sub>2</sub>H<sub>6</sub>) and the isotopic  
70 composition of CH<sub>4</sub> as tracers, can help attribute CH<sub>4</sub> emissions to O&G industry or other  
71 sectors (Röckmann et al., 2016; Lopez et al., 2017; Mielke-Maday et al., 2019; Maazallahi et al.,  
72 2020; Lu et al., 2021; Menoud et al., 2021; Gonzalez Moguel et al., 2022; Fernandez et al., 2022).  
73 Bottom-up approaches involve direct measurements of emissions usually at the source or  
74 component-level which are then extrapolated to larger scales using statistical methods.

75 The emission data reported to the United Nations Framework Convention on Climate  
76 Change (UNFCCC) for the year 2021 reveal that Romania ranks among the European Union  
77 (EU) countries with the highest annual CH<sub>4</sub> emissions from the O&G activities, following  
78 closely behind Italy and Poland. The International Energy Agency (IEA) estimates that  
79 Romania contributes the highest CH<sub>4</sub> emissions from the O&G industry among the EU-27  
80 countries (IEA, 2023). In light of the recent provisional agreement of EU methane regulations,  
81 which impose new requirements on the O&G industry for measuring, reporting, and mitigating  
82 CH<sub>4</sub> emissions (European-Commission, 2023), there is an urgent need to understand the extent  
83 and magnitude of emissions. This is particularly relevant for countries like Romania, where  
84 emissions are substantial but understudied, and addressing them is crucial for achieving EU  
85 climate objectives.

86 The ROMEO (ROmanian Methane Emissions from Oil and gas) project was designed  
87 to provide independent scientific measurement based CH<sub>4</sub> emission estimates for the O&G  
88 producing regions in Romania (Stavropoulou et al., 2023). The first phase of the ROMEO



89 campaign took place in October 2019, covering large production areas in southern Romania  
90 that are mostly associated with oil production. Numerous measurement techniques using a  
91 variety of instruments were deployed onboard ground-based and airborne measurement  
92 platforms. The data collected by vehicles and UAVs during the ROMEO campaign have  
93 already been evaluated separately in prior studies (Stavropoulou et al., 2023; Delre et al.,  
94 2022; Korbeň et al., 2022). Additionally, Menoud et al. (2022) investigated the isotopic  
95 signature of CH<sub>4</sub> emissions from the sites visited during the ROMEO campaign, contributing  
96 to insights in the reservoir characteristics.

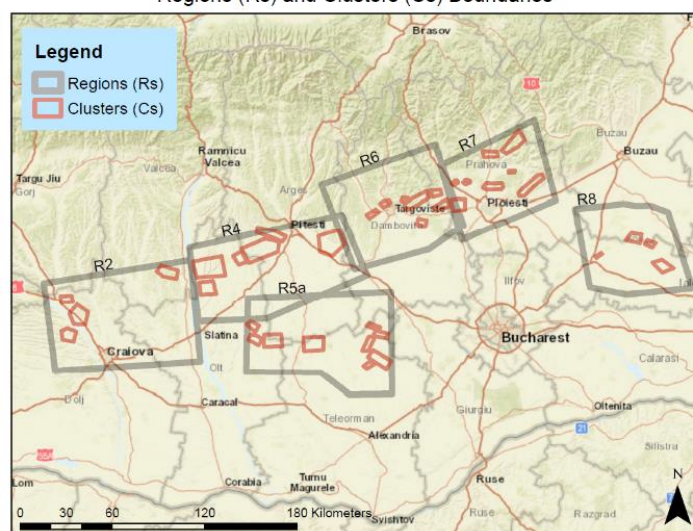
97 In this study, we present top-down CH<sub>4</sub> emission estimates derived from aircraft  
98 measurements of individual facilities, facility clusters, and extended regions during the  
99 ROMEO campaign. The measurements were performed by two research aircraft, and we used  
100 two mesoscale atmospheric chemistry and transport models to simulate atmospheric  
101 composition and transport over Romania.

## 102 2. Materials and methods

### 103 2.1. Clusters and regions

104 Information of O&G activities including locations, productions asset types, status and  
105 age of the facilities were received from the largest operator in the region. This information  
106 covers the majority of the total sites in the survey region, where other smaller operators are  
107 also present. The distribution of O&G production infrastructure in Romania is heterogeneous  
108 with a high density of production sites concentrated above the subsurface fossil fuel reservoirs.  
109 Therefore, we first grouped the installations in 40 clusters (Cs) and regions (Rs) (i.e.,  
110 aggregation of several production clusters). Both production clusters and regions were targets  
111 for the quantification approaches in the ROMEO campaign. Clusters are relatively small areas,  
112 usually a few to 20 km<sup>2</sup>, with a high density of O&G production sites. To derive basin-scale  
113 emission rates from aircraft measurements, the Romanian plain was further divided into larger  
114 regions of roughly 50 x 50 km<sup>2</sup>, which contain the clusters and are suitable for aircraft mass  
115 balance and raster flights.

Regions (Rs) and Clusters (Cs) Boundaries



Service Layer Credits: Sources: Esri, HERE, Garmin, USGS, Informa, INCREMENT P, NRCan, Esri Japan, METI, Esri China (Hong Kong), Esri Korea, Esri (Thailand), NGCC, (c) OpenStreetMap contributors, and the GIS User Community



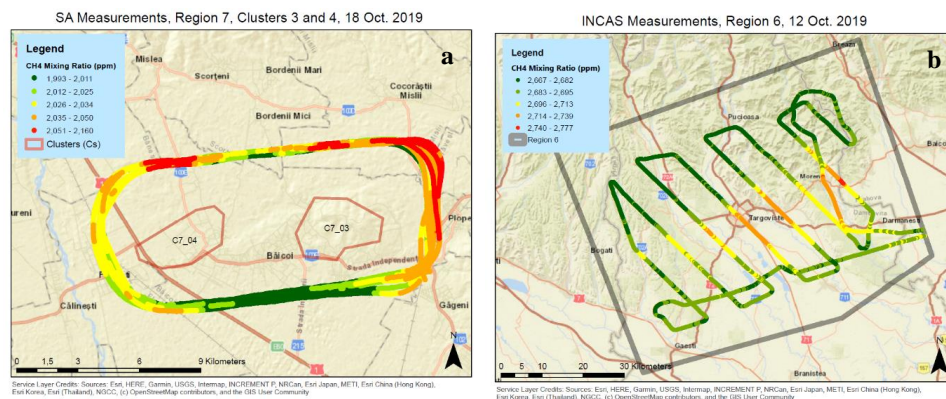
117 *Figure 1. Regions (grey polygons) and clusters (red polygons) that were targeted during the*  
 118 *ROMEIO 2019 campaign, circular or raster flights were performed within or around these*  
 119 *boundaries. Black symbols are individual sites of the O&G production infrastructure.*

120 **2.2. Aircraft-based in situ measurements**

121 Two aircraft were deployed during the ROMEIO 2019 campaign, a BN2 aircraft  
 122 operated by the National Institute for Aerospace Research "Elie Carafoli" (INCAS) and a two-  
 123 seater Mooney aircraft operated by Scientific Aviation (SA) Inc. On the Mooney aircraft, in-  
 124 situ measurements of CH<sub>4</sub>, C<sub>2</sub>H<sub>6</sub>, carbon dioxide (CO<sub>2</sub>), wind speed and direction, and relative  
 125 humidity were continuously logged at 1Hz frequency. C<sub>2</sub>H<sub>6</sub> and CO<sub>2</sub> were measured with  
 126 AERIS Pico Mobile LDS and Picarro G2301-f instruments and both instruments measured CH<sub>4</sub>  
 127 individually. On the BN2 aircraft, CH<sub>4</sub>, CO<sub>2</sub> and carbon monoxide (CO) were measured at  
 128 about 0.3 Hz frequency using a G2401 analyzer (Picarro Inc).

129 Two sets of flight patterns were performed, mass balance flights circling around target  
 130 areas (Fig. 2, left) and raster flights scanning the areas at a pre-selected observation density  
 131 (Fig. 2, right). During the 18 individual mass balance flights with the SA aircraft, the target  
 132 emission locations were circled at different altitudes to map the extent of the emission plume  
 133 (s), both vertically and horizontally. The emission rates were then calculated from the  
 134 measurements of CH<sub>4</sub> mole fraction and wind speed and direction in the mass balance approach  
 135 (see below). The BN2 aircraft was used to map possible emission sources over more extended  
 136 areas. The lack of wind measurements from this aircraft precludes a direct emission  
 137 quantification using the mass balance approach. These extended areas were surveyed in raster  
 138 patterns perpendicular to the prevailing wind (Fig. 2b). In addition to the identification of larger  
 139 sources, these measurements are also used to derive indirect emission rate estimates by  
 140 comparison to model simulations (see below).

141



142 *Figure 2 – Examples of a mass balance flight (a) and a raster flight (b) during the ROMEIO*  
 143 *2019 campaign. Black symbols are individual sites of the O&G production infrastructure. The*  
 144 *mass balance flight circled around two production clusters located in close proximity and the*  
 145 *raster flight covers a larger region. The color scale represents the CH<sub>4</sub> mole fraction.*  
 146

147 **2.3. Model simulations**

148 In order to support the emission quantification from the aircraft measurements, we  
 149 simulated atmospheric composition and transport over Romania using two numerical mesoscale  
 150 atmospheric chemistry and transport models: COSMO-GHG operated by the Swiss Federal  
 151 Laboratories for Materials Science and Technology (EMPA) and MECO(n) operated by the



152 German Aerospace Center (DLR). COSMO-GHG is based on the regional numerical weather  
153 prediction and climate model COSMO-CLM (Baldauf et al., 2011) and includes the GHG  
154 extension (Jähn et al., 2020; Brunner et al., 2019) for the simulation of (nearly) passive trace  
155 gases such as CH<sub>4</sub>. MECO(n) features an on-line coupling of the global chemistry-climate  
156 model EMAC with the regional chemistry-climate model COSMO-CLM/MESSy (Kerkweg  
157 and Jöckel, 2012). The COSMO-GHG simulations were nudged to the hourly wind data from  
158 the ERA5 reanalysis product of the European Centre for Medium-Range Weather Forecasts  
159 (ECMWF) (Hersbach et al., 2023). In MECO(n) the global model (EMAC) was nudged by  
160 Newtonian relaxation towards the operational analysis data from ECMWF (see (Nickl et al.,  
161 2020) for more details).

162 These two models were used to simulate the evolution of the CH<sub>4</sub> mole fraction arising  
163 from emissions from active O&G assets, including individual wells and larger facilities in time  
164 and space. For setting up the model simulations, each site was assigned an emission rate of 1 g  
165 s<sup>-1</sup> (3.6 kg hr<sup>-1</sup>). For COSMO-GHG, the model resolution was 2 x 2 km<sup>2</sup>, and the meteorological  
166 and compositional boundary conditions were provided from global scale modeling results  
167 obtained with the ECMWF/CAMS system. The MECO(n=3) set-up comprised four model  
168 instances (see (Klausner et al., 2020) for a detailed description of a similar model set-up). The  
169 first is the global model instance EMAC with a resolution of T42L90MA (corresponding to  
170 around 280 km spatial resolution). In the global model, three COSMO-CLM/MESSy instances  
171 were nested on-line with approx. 50 km resolution, approx. 7 km resolution, and the same 2 x  
172 2 km domain as applied for COSMO-GHG, respectively. In the applied MECO(3) set-up, we  
173 used a parameterized chemistry of methane (Winterstein and Jöckel, 2021) with monthly mean  
174 OH fields from previous simulations with comprehensive interactive chemistry. In the first,  
175 second, and third MECO(3) model instance we prescribed all anthropogenic and natural  
176 emissions of methane, in order to achieve realistic boundary conditions of methane for the finest  
177 resolved instance. In this instance the emissions were used as described below. The model  
178 outputs provide atmospheric CH<sub>4</sub> mole fractions fields as well as meteorological parameters at  
179 a temporal resolution of 20 min (COSMO-GHG) and 1 hr (MECO(3)). For MECO(3), only the  
180 results of the finest instance are considered here for further analysis. To be able to attribute  
181 emissions to certain emission clusters, we transported 33 individual “CH<sub>4</sub> tracers” based on 3  
182 inventories. 21 of these tracers represent the emissions of individual clusters and regions, and  
183 in some cases even represent gas and oil emissions separately. To limit the number of tracers,  
184 one tracer represents the emissions of one or two clusters and one or two distant regions,  
185 assuming that they are sufficiently far away. This allows us to separate the signal of each cluster  
186 flown over or circled around.

#### 187 **2.4. Emission inventories**

188 To drive the simulations and interpret the data we use information from various  
189 emission inventories. (1) The most granular dataset is based on information on the production  
190 infrastructure provided by the oil and gas operator. It consists of about 6000 individual  
191 production-related locations in the Southern part of Romania. We will refer to this dataset as  
192 the “O&G\_operator” dataset. In order to convert this to an approximate emission inventory, we  
193 divided reported emissions for Romania by the number of emission locations and assigned the  
194 result as average emission rate to all of these locations. Coincidentally, this average value is  
195 close to 1 g s<sup>-1</sup> site<sup>-1</sup> (3.6 kg hr<sup>-1</sup> site<sup>-1</sup>), which was used as prior emission rate in the model  
196 simulations. (2) The TNO\_GHGco inventory (Denier van der Gon et al., 2018) includes  
197 emissions from all available sectors at 5 km x 5 km resolution. (3) The European Pollutant  
198 Release and Transfer Register/Industrial Emissions Directive (E-PRTR/IED) inventory (E-  
199 PRTR, 2023) includes major point sources and was used to identify major farm and landfill  
200 methane emitters within the study areas (Figure S2 in the SI). (4) The TNO - Copernicus



201 Atmospheric Monitoring Service European Regional Inventory (TNO-CAMS) (Kuenen et al.,  
202 2022) and (5) the Emissions Database for Global Atmospheric Research (EDGAR, 2023)  
203 inventories were used to calculate the percentage of O&G emissions to total emissions in the  
204 target areas.

205 In summary, based on TNO-CAMS no coal mine locations, a potentially large source  
206 of CH<sub>4</sub>, were identified within the mass balance flight boundaries. The presence of major  
207 wetlands was investigated based on the findings of Saarnio et al. (2009) and no wetlands were  
208 observed within the measured areas.

## 209 **2.5. Analysis of simulated meteorological quantities**

210 The meteorological conditions during the ROMEO campaign were not ideal for  
211 emission quantification due to the low wind speeds. This complicated the use of a model –  
212 measurement comparison for the raster flights, which we had planned to use to derive  
213 quantitative emission information. To assess the model performance in terms of meteorological  
214 conditions during the individual flight days, we compared the meteorological output of the  
215 models with each other, with ERA5 reanalysis data, and with the meteorological information  
216 recorded during the Scientific Aviation flights. The rationale is: when the models do not agree  
217 on the general meteorological conditions in a target region, we also expect diverging CH<sub>4</sub>  
218 concentration distributions, which would hamper quantitative comparison to the measurements.  
219 On the other hand, when the meteorological conditions are simulated consistently, there is more  
220 confidence that the transport is simulated adequately as well, thus the simulated and observed  
221 CH<sub>4</sub> plumes may be used to derive emission information.

222 For each flight date, the following parameters were investigated in each flight region:  
223 temperature, cloud fraction, wind speed and direction, specific humidity, and relative humidity.  
224 Based on selected threshold values, the meteorological parameters for each model and each  
225 flight day were characterized as good, acceptable, or poor. Furthermore, we evaluate three  
226 quantitative indices, the Nash - Sutcliffe Efficiency (NSE), the Kling-Gupta Efficiency (KGE),  
227 and the Mean Absolute Relative Error (MARE) between simulation results and ERA5  
228 reanalysis data. The results of this comprehensive analysis are presented in the Supplementary  
229 Information (SI).

## 230 **2.6. Emission quantification: Mass balance approach**

231 CH<sub>4</sub> emission rates from 11 production site clusters (or combinations of clusters), three  
232 larger regions in the Romanian Basin, and two groups of individual sites were quantified from  
233 aircraft-based measurements using the mass balance approach. This approach is based on the  
234 Gaussian theorem in which the difference of the total fluxes into and out of an enclosed area  
235 must be balanced by a source or sink in the area (Conley et al., 2017). CH<sub>4</sub> enhancements were  
236 identified using background values determined either from the upwind flight legs or from the  
237 edges of detected plumes.

238 The mass balance approach returns total CH<sub>4</sub> emissions for the target areas. For the  
239 intense production clusters, the emissions are in most cases dominated by the O&G production  
240 infrastructure. Therefore, we assigned 100% of the emissions in the clusters to O&G  
241 production, except for clusters which contained a landfill and/or large farm, as included in the  
242 E-PRTR inventory. In particular, only one significant landfill was identified in R6C6, and the  
243 emissions reported from this landfill were deducted from the measured flight quantification.  
244 For the larger areas, the contributions from other sectors can be substantial. To infer emissions  
245 related to O&G operations from the total measured emissions, we estimated the emissions from  
246 non-O&G sources in the target areas using the TNO-CAMS inventory and subtracted these  
247 from the total measured emissions. We repeated the same process using the EDGAR inventory.



248 These O&G related emissions were then divided by the number of active O&G infrastructure  
249 elements in the target area to derive an emission factor per site for that cluster or region. This  
250 includes active production sites, processing sites, compressor stations, and other active sites,  
251 which all contribute to the measured emissions. Possible emissions of non-producing sites are  
252 not included in our estimates, as they are likely smaller (on average) than the ones of producing  
253 sites.

## 254 **2.7. Emission quantification: Measurement - model comparison**

### 255 **2.7.1. Mass balance flights**

256 The simulated CH<sub>4</sub> distributions were evaluated along the flight tracks in order to  
257 facilitate direct comparison with the observations. For the mass balance flights (Fig 2a), the  
258 lowest CH<sub>4</sub> value of each circle around a target area was defined as background mole fraction  
259 and subtracted from downwind measurements to obtain the CH<sub>4</sub> enhancement. To compare  
260 model and measurement results, we integrated the CH<sub>4</sub> enhancement above background along  
261 the flight track for each circle, both for the measurements and for the simulated CH<sub>4</sub> mole  
262 fractions along the flight tracks. These integrals are referred to as plume areas. Circles that were  
263 identified as influenced by up-stream contamination were excluded from the analysis. The  
264 simulated plume areas were then plotted versus the measured plume areas, and the slope of the  
265 orthogonal linear regression line returns a measurement-based scaling factor to the prior  
266 emission rate estimate that was in the simulations (1 g s<sup>-1</sup> site<sup>-1</sup>). This scaling factor was then  
267 assigned to the active O&G facilities in the target cluster or region and provides a measurement-  
268 based estimate of the emission factor.

### 269 **2.7.2. Raster flights**

270 For the raster flights (Fig. 2b), the lowest CH<sub>4</sub> mole fraction along the flight track across  
271 a target region was defined as background and the CH<sub>4</sub> enhancements above this background  
272 were integrated. The simulations were treated in the same way. The slopes of the orthogonal  
273 linear regressions between integrated enhancements from flight measurements and simulations  
274 were then compared to the scaling factors determined from the mass balance flights (2.7.1) to  
275 investigate whether the model – observation slopes are consistent between individual plumes  
276 and the raster flights over larger regions. The rationale is that even if the quantitative modeling  
277 is challenging under the encountered meteorological conditions, if the slopes derived from the  
278 mass balance and raster flights are comparable, then the emission factors derived from the mass  
279 balance flights should be also representative for the larger regions covered by the raster flights.

## 280 **3. Results and discussion**

### 281 **3.1. Mass balance quantifications**

282 Table 1 shows the results of the emissions quantifications obtained from mass balance  
283 calculations using the measurements of the SA aircraft. Methane emission rates range between  
284 tens of kg hr<sup>-1</sup> from an individual facility or smaller cluster up to more than 8000 kg hr<sup>-1</sup> for the  
285 larger region R7 which includes the city of Ploiesti. These emissions are representative of the  
286 sum of all sources in each target area. Especially the larger regions include emissions from other  
287 sectors, particularly agriculture and waste. On the other hand, the CH<sub>4</sub> in the dense production  
288 clusters originate to nearly 100% from O&G activities.

289 Different inventories (E-PRTR, TNO-CAMS and EDGAR) were consulted to obtain  
290 information about the non-O&G contributions; however, these inventories are generally not  
291 designed to distribute emissions across sectors on such small scales. TNO-CAMS and EDGAR  
292 have a coarse spatial resolution and do not include production clusters, so they are not suitable  
293 to assess the emissions distribution across sectors in such clusters. With the exception of R6C6,



294 which includes a landfill listed in E-PRTR, for all other production clusters, E-PRTR does not  
295 indicate any major farms or landfills. The ground teams did not observe significant non-O&G  
296 sources in the smaller production clusters. Therefore, we ascribe 100% of the total emissions in  
297 clusters to O&G production. For the large regions R7 and R5a, we use the estimated absolute  
298 non-O&G emissions from TNO-CAMS and subtract them from the measured emissions to  
299 correct for non-O&G related emissions.

300 The emission factors (EF) provided in Table 1 are calculated using the number of total  
301 active (e.g. producing, or operating) infrastructure elements within the target regions, because  
302 the measurements do not allow us to distinguish between different parts of the infrastructure.  
303 The emission factors vary widely among the individual clusters, from 1.0 to 20 kg hr<sup>-1</sup> site<sup>-1</sup>.  
304 This is partly due to the inhomogeneous distribution of the emissions, where few sites are  
305 responsible for a large share of the emissions. A contributing factor is that each quantification  
306 yields an emission estimate for the specific moment in time of the measurement. The variability  
307 in our cluster-specific emission factors may partly represent the episodic tendency of O&G  
308 super-emitters. However, given the generally large number of infrastructure elements within  
309 the target regions, the reported numbers should still reflect representative averages for the  
310 clusters and regions, also over longer periods. Note that the timing of our measurements is  
311 random, and the total facility sample size (N=4358, including duplicates, see below) is large.  
312 To address the challenge of emissions' variability and inhomogeneity, we employ a weighted  
313 averaging approach based on facility numbers.

314 Table 1 shows that over all mass balance flights around production clusters and larger  
315 regions, a total of roughly 31,700 kg hr<sup>-1</sup> of CH<sub>4</sub> emissions were quantified. Dividing this by  
316 the number of active facilities in the target regions (4358) would lead to an emission factor of  
317 7.3 kg hr<sup>-1</sup> site<sup>-1</sup>. However, this number is biased high for two reasons: i) not all of the measured  
318 emissions originate from the O&G production facilities, in particular for the large regions, and  
319 ii) there is some “double” or even “triple counting” of sites. Specifically, the emission from the  
320 larger regions R5a and R7 were quantified twice, and the sites in the quantified clusters of R7  
321 contribute to the emissions from the clusters and the regional flights. Note that the activity  
322 factors are also counted several two or three times in this case, so the calculations are still valid,  
323 but sites that are quantified multiple times have more weight in calculation of the EF.

324 To exclude double or triple counting emissions from the same facilities, we estimate an  
325 EF based solely on the larger region quantifications for R5a and R7. In the case of regions R4,  
326 R8 and R6 where no regional quantification was performed or regional quantifications were  
327 unsuccessful, we aggregate the emissions from the individual production clusters. When we  
328 remove the double counting and account for emissions from other sources as explained above,  
329 the total emissions quantified over these mass balance flights are 13,216 ± 4932 kg hr<sup>-1</sup>, which  
330 results in a facility-weighted emission factor of 5.3 ± 2.0 kg hr<sup>-1</sup> site<sup>-1</sup>. We note that these  
331 estimates from the mass balance flights represent a large fraction of the O&G infrastructure in  
332 the Southern Romanian region (2516 total sites, Table 1) and are thus statistically representative  
333 of the area.

334 By design, regions with more sites contribute more to facility-weighted emission factors  
335 than regions with less sites. In our case, region R5a has nearly twice as many facilities as the  
336 next most densely populated region and thus carries the largest weight in the calculations. We  
337 recall that the weather conditions during the ROMEO campaign were not ideal for large scale  
338 mass balance quantifications. It is possible that the area mass balance quantifications in the flat  
339 and arid region R5a in Southern Romania may be biased slightly low due to partial loss of CH<sub>4</sub>  
340 out of the boundary layer during the hot and convective conditions, or due to the fact that stable  
341 transport conditions had not yet established over the large regions (e.g. not all emissions in the





342 region had time to leave through the downwind edge where the measurements took place). In  
343 addition, the results from the region R5a flights were affected by upwind emissions.

344 For flights around dense production clusters with 100% O&G contribution, the  
345 weighted average emissions factor is  $4.4 \pm 1.7 \text{ kg hr}^{-1} \text{ site}^{-1}$ . This aligns with the estimate from  
346 the large regions within the uncertainty ranges (EF of  $5.3 \pm 2.0 \text{ kg hr}^{-1} \text{ site}^{-1}$ , Table 1),  
347 considering the differences in the number of facilities included in each estimate ( $N=1570$  for  
348 the clusters and  $N=2516$  for the large regions). These estimates also agree within the errors with  
349 the  $5.4 (3.6 - 8.4) \text{ kg hr}^{-1} \text{ oil production site}^{-1}$  (95% CI:  $3.6 - 8.4$ ) reported from the ground-  
350 based measurements by Stavropoulou et al. (2023) for oil production sites. The estimate derived  
351 from the cluster flights encompasses a total of 1570 facilities, compared to up-scaling from  
352 about dedicated measurements at 178 oil production sites in Stavropoulou et al. (2023). The  
353 emissions quantified with the aircraft include all facilities in a certain region or cluster, not only  
354 the production facilities. Other facilities include facilities that may emit more than an individual  
355 well (e.g. oil parks) but also facilities that emit less (e.g. injection or disposal facilities). If the  
356 co-produced gas from oil production sites is already vented at the production sites as reported  
357 in (Stavropoulou et al., 2023), then the production sites may indeed be larger emitters than the  
358 average, because most of the gas already escapes at the production site.

359 As the campaign airport was located close to the city of Ploiesti in region R7, the  
360 majority of cluster quantifications were carried out in R7 for logistical reasons and many of the  
361 dense production clusters in R7 were quantified. This allows us to compare the sum of the  
362 emission rates determined from cluster quantifications to the emission factors from regional  
363 quantifications. The cluster flights in region R7 quantified a total of 377 O&G sites, which is  
364 75% of the 500 sites that were quantified in the regional flights. The quantified emissions from  
365 the cluster flights ( $3828 \pm 1199 \text{ kg hr}^{-1}$ ) amount to 54% of the total emissions quantified in the  
366 regional flights, after subtracting non-O&G emissions (about  $7038 \pm 1769 \text{ kg hr}^{-1}$  from two  
367 independent flights, Table 1). This indicates a possible underestimate of non-O&G emissions  
368 in the inventories for R7, which includes the large city of Ploiesti. Alternatively, some super-  
369 emitters may exist outside the quantified clusters, which would increase the regional estimate.  
370 Nevertheless, the region and cluster flights show a reasonable level of consistency in region  
371 R7. The emission factors further support this alignment, with the weighted sum of the clusters  
372 being equal to  $10.2 \pm 3.2 \text{ kg hr}^{-1} \text{ site}^{-1}$  compared to about  $14.1 \pm 3.6 \text{ kg hr}^{-1} \text{ site}^{-1}$  for the regional  
373 flights.

374 The aircraft-based quantifications indicate that per-site emission factors from region R7  
375 are higher than from the other regions. At the same time, R7 was best covered in terms of mass  
376 balance determinations, so it is the most reliable estimate. From the site-level quantifications  
377 carried out on the ground, it was not apparent that per-site emission rates varied between  
378 different regions (Stavropoulou et al., 2023; Delre et al., 2022; Korbeń et al., 2022).

379 When we use the derived emission factor of  $5.3 \pm 2.0 \text{ kg hr}^{-1} \text{ site}^{-1}$  and scale this up to  
380 the entire production basin in Southern Romania with more than 4900 active sites, annual  
381 estimated emissions estimated at  $227 \pm 86 \text{ kt CH}_4 \text{ yr}^{-1}$ . If the derived EF also applies to the  
382 infrastructure in other parts of Romania the inferred country-scale emission rate from about  
383 7400 active sites in 2019 is  $344 \pm 130 \text{ kt CH}_4 \text{ yr}^{-1}$ . Reported emissions to the UNFCCC for  
384 Romania in the category *1.B: Fugitives* include  $53 \text{ kt CH}_4 \text{ yr}^{-1}$  for activity *1.B.2.b Natural Gas*,  
385  $38.2 \text{ kt CH}_4 \text{ yr}^{-1}$  for *1.B.2.c Venting and Flaring (oil, gas, combined oil and gas)* and  $10.4 \text{ kt yr}^{-1}$   
386 for *1.B.2.a Oil* (UNFCCC, 2023b). This adds up to  $101.6 \text{ kt CH}_4 \text{ yr}^{-1}$ , about 3 times less than  
387 our estimate. Our estimate does not include emissions from infrastructure operated by other  
388 operators, for example the large gas production region in the Transylvanian Basin. An intensive  
389 ground-based study has been carried out there and the results are in preparation for publication  
390 (Jagoda et al., in preparation, 2024).



391 For comparison, we repeated the analysis using the EDGAR inventory to estimate non-  
 392 O&G sources for the large regions (see SI, Table S6). After removing double counting and  
 393 adjusting for emissions from other sources as described previously, the total emissions  
 394 measured attributed to O&G production are  $12,732 \pm 4932 \text{ kg hr}^{-1}$ . This is slightly lower than  
 395 the total emissions estimated using the TNO-CAMS inventory  $13,216 \pm 4932 \text{ kg hr}^{-1}$ , indicating  
 396 a larger fraction of non-O&G sources in the EDGAR inventory. The inferred O&G emissions,  
 397 taking into account the non-O&G emissions from the EDGAR inventory result in a facility-  
 398 weighted emission factor of  $5.1 \pm 2.0 \text{ kg hr}^{-1} \text{ site}^{-1}$ , consistent with the  $5.3 \pm 2.0 \text{ kg hr}^{-1} \text{ site}^{-1}$   
 399 when using TNO-CAMS for the non-O&G sectors. It is important to note that the inventory  
 400 estimates for the non-O&G sectors do not differ strongly between EDGAR and TNO-CAMS  
 401 in the regions where we apply the corrections. However, this is not the case for all regions in  
 402 the southern Romanian production basin. Table S7 in the Supplement shows that the  
 403 discrepancies between the two inventories can become large. Specifically, in EDGAR, the non-  
 404 O&G emissions are higher than those in TNO-CAMS, nearly double in some cases. Moreover,  
 405 O&G emissions are very low in EDGAR, whereas they contribute to almost half of the  
 406 emissions in TNO-CAMS. Because of this more balanced contribution from all sources, we use  
 407 the estimates from TNO-CAMS for our central emission factor estimate and for the upscaling.

408 *Table 1 - Measured emission rates (ER) and estimates of the O&G related fraction of total CH<sub>4</sub>*  
 409 *emissions in target regions and clusters. “Non-O&G emissions (kg hr<sup>-1</sup>)” are extracted from*  
 410 *the TNO-CAMS inventory for the target regions and are used to derive ERs from the O&G*  
 411 *industry in the area (“O&G emissions”). The last column shows the emission factor (kg CH<sub>4</sub>*  
 412 *hr<sup>-1</sup> site<sup>-1</sup>). Numbers in bold are used for upscaling to the national scale (see text for details).*

Flight ID	Target region/cluster	# facilities	# wells	Total Measured Emissions (kg hr <sup>-1</sup> )	Non-O&G emissions (kg hr <sup>-1</sup> )	O&G emissions (kg hr <sup>-1</sup> )	EF (kg h <sup>-1</sup> site <sup>-1</sup> )
SA01	R7	496	337	8517 ± 2097	1388	7129 ± 2097	14.4 ± 4.2
SA02	R7	504	343	8335 ± 1440	1388	6947 ± 1440	13.8 ± 2.9
SA03	R5a	827	654	4556 ± 2570	772	3784 ± 2570	4.6 ± 3.1
SA04	R5a-small	818	642	2920 ± 935	374	2516 ± 935	3.1 ± 1.1
SA05	R6C2C3C4	471	379	1729 ± 912	-	1729 ± 912	3.7 ± 1.9
SA06	R7C3C4	124	92	1481 ± 287	-	1481 ± 287	11.9 ± 2.3
SA07	R7C2	71	44	1395 ± 546	-	1395 ± 546	19.6 ± 7.7
SA08	R7VentArea	67	41	602 ± 209	-	602 ± 209	9.0 ± 3.1
SA09	R4C5	390	347	477 ± 106	-	477 ± 106	1.2 ± 0.3
SA10	R6C6	29	16	469 ± 170	130†	339 ± 170	11.7 ± 5.9
SA11	R7Vent	37	20	266 ± 113	-	266 ± 113	7.2 ± 3.1
SA12	R7C5	59	45	259 ± 47	-	259 ± 47	4.4 ± 0.8
SA13	R4C2C3	247	186	246 ± 89	-	246 ± 89	1.0 ± 0.4
SA14	R6C5	27	21	131 ± 85	-	131 ± 85	4.9 ± 3.1
SA16	R8C1	29	19	90 ± 49	-	90 ± 49	3.1 ± 1.7
SA17	R7C8	48	43	78 ± 101	-	78 ± 101	1.6 ± 2.1
SA18	R7C1Facility	8	5	13 ± 9	-	13 ± 9	1.6 ± 1.1
Weighted mean, everything		4358	3303	31667 ± 10039	*, †	27513 ± 9765	6.3 ± 2.2



No double counting	2516	1956		*, †, ††	<b>13216 ± 4932</b>	<b>5.3 ± 2.0</b>
Sum of clusters in R7	377	270			3828 ± 1199	10.2 ± 3.2
Only clusters with 100% fossil	1570	1238			6970 ± 2610	4.4 ± 1.7

\* considering the absolute non-O&G emissions from the TNO-CAMS inventory for the large regions and 100% O&G contribution for the clusters

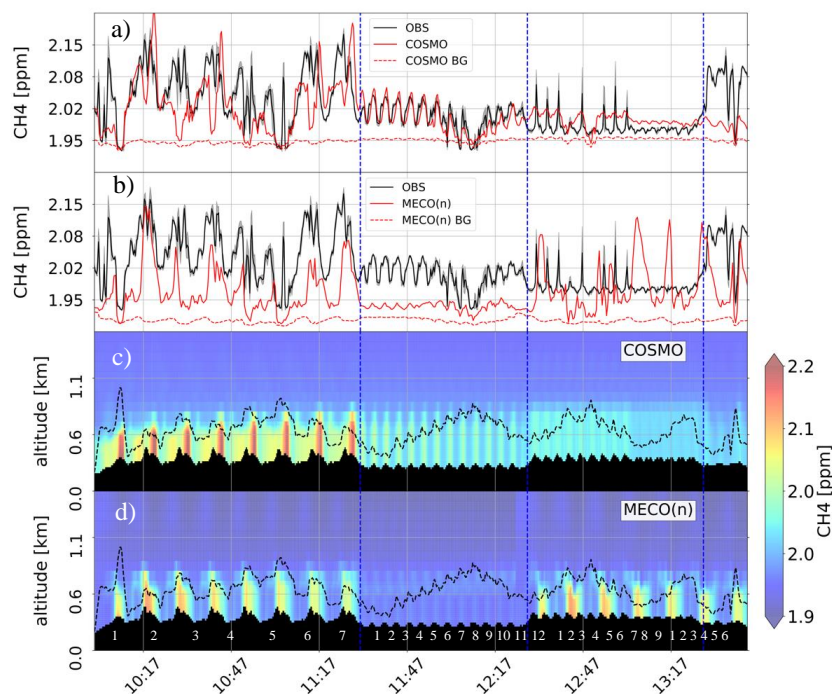
† accounting for landfill within R6C6

†† excluding cluster quantifications in R7

### 413 3.2. Qualitative information from measurement - simulation comparisons

#### 414 3.2.1. Example comparison of meteorology and CH<sub>4</sub> for a mass balance flight

415 Figure 4 shows an example of a comparison between measurements along the SA mass  
 416 balance flight from October 17, 2019, with results from the COSMO-GHG and MECO(3)  
 417 models. The top two panels show simulated and measured CH<sub>4</sub> mole fractions along the flight  
 418 track and the bottom two panel shows the vertical CH<sub>4</sub> profiles in the simulations along the  
 419 flight track above the changing orography (black). During this flight, 4 different clusters and  
 420 combinations of clusters were circled multiple times at different altitude; the flight altitude is  
 421 included in the bottom panels as dashed black line. The repeating orographic patterns guide the  
 422 eye in following the circular flight patterns around the clusters and are numbered in white. The  
 423 colored contours illustrate the vertical CH<sub>4</sub> profiles along the flight track. The measured plume  
 424 in the first, largest, cluster is captured relatively well by the simulation for some of the cycles,  
 425 but during some cycles the flight track is partly above the boundary layer in the models and the  
 426 peak is not fully captured. During cycles 4 and 5, the observations suggest that the aircraft was  
 427 flying above the boundary layer also in reality, but one sharp, narrow peak was still observed  
 428 after the highest orographic peak in the measurements, which is missing in the simulation. For  
 429 the second cluster that was cycled 12 times, the COSMO-GHG model captures the plumes  
 430 better than the MECO(3) model. For both models, the simulated and measured CH<sub>4</sub> mole  
 431 fractions show a consistent transition out of the boundary layer in cycles 7-9, indicating a good  
 432 representation of the boundary layer height in the models. For the third cluster, the models are  
 433 missing the large, sharp peaks, indicating missing emissions in this cluster. In addition, the  
 434 MECO(3) model simulates higher plumes when the flight track was in the model boundary  
 435 layer, but lower plumes when the flight track was outside the boundary layer. For the last  
 436 cluster, the simulated and measured elevations are small and relatively consistent for COSMO-  
 437 GHG, but the MECO(3) model simulates some larger plumes spanning more than one cycle,  
 438 indicating larger scale upwind contamination, which was also documented in the observations.



439  
 440 *Figure 3 – Measurements and simulation results of (a&b) CH<sub>4</sub> mole fraction along the flight*  
 441 *track, and (c&d) the vertical CH<sub>4</sub> profile along the flight track as simulated by the COSMO*  
 442 *model (a&c) and the MECO(3) model. Model background fields are shown as dashed lines in*  
 443 *a&b. Panel c&d also include the flight track as black dashed line, and the black contour at the*  
 444 *bottom shows the orography in this mountainous terrain; the repeating patterns illustrate*  
 445 *individual cycles around the clusters R6C2C3C4, R6C5, R6C6 and R6C7, cycles are numbered*  
 446 *in white. The flight around cluster R6C7 did not allow successful emission quantification*  
 447 *because of an upwind influence and is therefore not included in Table 1.*

448 A similar analysis was performed for each flight with the goal to identify plumes where either  
 449 the simulation results or the measurements indicated that the respective circle was flown outside  
 450 the simulated or actual boundary layer. In this case, the respective plume was not retained for  
 451 the measurement – simulation comparison. In total, 10 out of 200 individual plumes were  
 452 rejected this way. In addition, 66 circles around clusters that were influenced by signals from  
 453 upwind sources were excluded.

### 454 3.2.2. Model performance in terms of meteorology

455 As mentioned above, the low winds during the campaign period presented difficult  
 456 meteorological conditions for emissions quantification. We performed a thorough  
 457 meteorological analysis to identify days when the meteorological conditions agree well between  
 458 the two models and the measurements. The results are shown in S.1 in the SI, which illustrate  
 459 that it was not possible to identify days when the meteorological conditions agree well between  
 460 the two models and the measurements. Therefore, it was decided not to focus on individual days  
 461 or flights. Rather, in the following we compare the measured and simulated plume areas  
 462 statistically across all available flights. This is done to investigate whether correlation of  
 463 measured and simulated CH<sub>4</sub> enhancements from the raster flights, which cover a wider region,



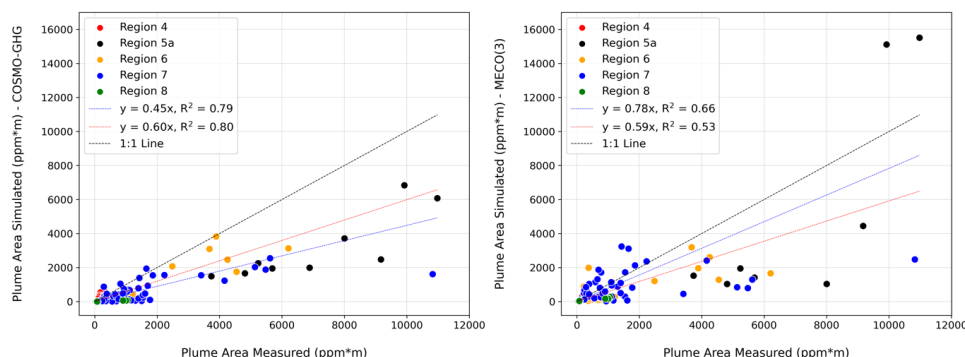
464 is similar to the one for the individual plumes quantified during the mass balance flights. The  
 465 analysis, which is described in the section below, can also possibly identify regional differences  
 466 and be used to derive approximate scaling factors for the raster flights in comparison with the  
 467 mass balance flights.

### 468 3.3. Measurement - model comparison of plume areas for mass balance flights

469 We first evaluate individual plume-level data from the mass balance flights, because for  
 470 these flights we have measured emission rates from the mass balance approach. Thus, we can  
 471 compare the measured and simulated plume areas and derive a correction factor for the emission  
 472 rates assumed in the model that would bring the measured and simulated plumes to agreement.  
 473 Fig. 4 shows the comparison of the observed and simulated plume areas for 190 individual  
 474 plumes evaluated from the SA mass balance flights and COSMO-GHG and MECO(3) models,  
 475 respectively.

476 For mass balance flights around production clusters, each circle around a cluster results  
 477 in one or few down-wind plumes (which are integrated in our analysis), but for mass balance  
 478 flights targeting larger regions, numerous well-separated plumes can generally be quantified  
 479 from a single circle. The high scatter in the comparison between simulated and measured plume  
 480 areas can be ascribed to a number of factors, for example: i) large variability in actual emissions  
 481 from different source areas (here: production clusters), including the important role of super  
 482 emitters, ii) difficult meteorological conditions with low wind leading to variable plume  
 483 representations, both in the real atmosphere and in the model, iii) over- or underestimates  
 484 associated with the dynamics of the planetary boundary layer, and iv) variable measurement  
 485 distance from the emission points. The scatter in the comparison of plume areas with MECO(3)  
 486 results is even larger than for the COSMO-GHG model. This is ascribed to the fact that the  
 487 meteorological fields in COSMO-GHG are nudged to observations, whereas MECO(3) nudges  
 488 only the global model instance, implying more degrees of freedom within the nested instances  
 489 to develop their own (sub-synoptic) meteorological situation which might deviate from the data  
 490 used for nudging. Indeed, the meteorological evaluation (See S.1 in the SI) shows that the  
 491 meteorological fields in COSMO-GHG (directly nudged) are closer to the observed  
 492 meteorological parameters than for MECO(3), as expected.

493



494

495 *Figure 4 - Comparisons between plume areas calculated from measurements and simulations*  
 496 *with COSMO-GHG (left) and MECO(3) (right). Blue dashed lines show linear fits to all data*  
 497 *and red dashed lines linear fits to the plumes from the clusters only, without the points from*  
 498 *the larger regions. Plots zooming in on the region of plume areas up to 2000 ppm \* m are*  
 499 *shown Figure S1 in the SI.*

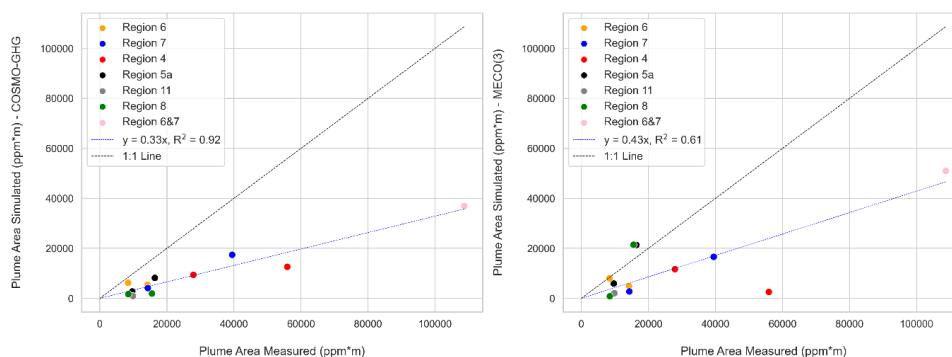


500 Nevertheless, despite the variability, it is evident that most of the points fall well below  
501 the 1:1 line, which means that the simulated plume areas along the flight track that were  
502 generated with an assumed emission factor of  $1 \text{ g s}^{-1} \text{ site}^{-1}$ , thus  $3.6 \text{ kg hr}^{-1} \text{ site}^{-1}$ , generally  
503 underestimate the measured plume areas. The further the points fall below the 1:1 line, the  
504 higher the implied mismatch in the emission rate that was assumed in the model. A linear fit to  
505 all the measured and simulated plumes has a slope of 0.44 for COSMO-GHG, and 0.78 for  
506 MECO(3). When we exclude the points from the larger regions, where the measured plumes  
507 are often further away from the source regions, the slopes change slightly to 0.56 for COSMO-  
508 GHG, and to 0.62 for MECO(3). This suggests that the assumed emission rate in the model is  
509 on average underestimated by about a factor of 2. However, quantitative interpretation is  
510 problematic in this approach, since the slope of the linear fit is largely determined by a relatively  
511 small number of plumes with large plume areas. Furthermore, the sampling is biased towards  
512 clusters where more circles were flown (i.e., circles at more altitude levels), and does not  
513 consider the number of facilities per cluster. In addition, there may be systematic biases in the  
514 models, e.g. due to model resolution or meteorological conditions (as discussed above), that  
515 lead to smaller plume areas in the models compared to the measurements. For the present  
516 purpose, we will compare the slope of observed and simulated plume areas from the mass  
517 balance flights determined here with the slope of observed and simulated  $\text{CH}_4$  enhancements  
518 from the raster flights in section 3.4.2 to investigate whether the enhancements observed during  
519 the raster flights qualitatively agree with the ones from the mass balance flights.

### 520 **3.4. Measurement - model comparison of plume areas for raster flights**

521 Figure 5 shows the comparison of the integrated enhancement above background along  
522 the flight tracks for  $\text{CH}_4$  mole fractions measured during the raster flights and simulated with  
523 the two models. The scatter for these integrated enhancements is smaller than for the individual  
524 plume areas shown in Fig 4., which likely reflects the fact that the integrated enhancements are  
525 the sum of numerous plumes, and high and low values average out for the integrated  
526 enhancements.

527 Similar to the plume area comparison from the mass balance flights (Fig. 4), most of the  
528 points fall below the 1: 1 line, again indicating that the emission rate of  $3.6 \text{ kg hr}^{-1} \text{ site}^{-1}$  assumed  
529 in the models is insufficient to explain the observed concentrations. The slopes of the  
530 orthogonal linear regressions of 0.43 and 0.33 for the two different models are even lower than  
531 for the mass balance flights above, indicating a possible underestimate by up to a factor of 3 in  
532 the assumed emission rate. Still, the slopes are in a similar range as the slopes from the mass  
533 balance flights in Fig. 4. It is important to note that these slopes were now derived from the  
534 simulated fields under similar conditions as the ones for the individual plumes from the clusters.  
535 Thus, whereas various factors could cause systematic under- or overestimates in simulated  
536 versus measured  $\text{CH}_4$  enhancements, the similar slopes obtained for the two types of flights  
537 suggest that the emission characteristics of the plumes observed during the mass balance and  
538 raster flights are compatible. Thus, the emission factors derived for a limited number of clusters  
539 in section 3.3 are likely representative for the larger areas covered in the mass balance flights,  
540 and thus for a large fraction of the Southern Romanian O&G production infrastructure. We  
541 conclude that the  $\text{CH}_4$  enhancements observed on the BN2 aircraft during the raster flights  
542 generally support the emission factors derived in section 3.1 from the mass balance approach.



543  
 544 *Figure 5 - Comparison between integrated CH<sub>4</sub> enhancements from measurements during*  
 545 *raster flights on the BN2 aircraft, and simulations along the flight tracks with COSMO-*  
 546 *GHG (left) and MECO(3) (right). Different colors represent different regions. Linear fits to*  
 547 *the data are shown as blue dashed lines and the 1: 1 line is shown as black dashed line.*

548 **4. Conclusions**

549 Airborne measurements of methane performed from two aircraft during the ROMEO  
 550 2019 campaign were evaluated to obtain emission rate estimates representative for production  
 551 clusters and larger regions in the O&G production basin in Southern Romania. Emissions  
 552 determined from a mass balance approach yield a wide range of instantaneous emission factor  
 553 estimates between different clusters, supporting the heterogeneity of emissions across  
 554 individual sites, regions and time. Assessment of the O&G emissions from flights around larger  
 555 regions is difficult because of the unknown contribution of emissions from other sectors. From  
 556 mass balance estimates covering a total of 2516 sites, using the TNO-CAMS inventory to derive  
 557 emissions from non-O&G sources for the large regions, and assuming 100% of the observed  
 558 emissions in the smaller clusters to originate from O&G production, we derive total emissions  
 559 of  $13,216 \pm 4932 \text{ kg hr}^{-1}$  for the covered regions in Southern Romania. This results in a facility-  
 560 weighted emission factor of  $5.3 \pm 2.0 \text{ kg hr}^{-1} \text{ site}^{-1}$ , consistent with the previously published  
 561 estimate from ground-based quantifications of  $5.4 \text{ kg hr}^{-1} \text{ oil production site}^{-1}$  (range  $3.6 - 8.4$   
 562  $\text{kg hr}^{-1} \text{ site}^{-1}$ , (Stavropoulou et al., 2023). The facility-weighted average for 1570 facilities in  
 563 dense production clusters, where we are certain that the dominant contribution is from the O&G  
 564 infrastructure is  $4.4 \pm 1.7 \text{ kg hr}^{-1} \text{ site}^{-1}$ , aligning with the estimate from larger regions. Using  
 565 the of  $EF 5.3 \text{ kg hr}^{-1} \text{ site}^{-1}$  to scale up to the national scale results in an annual emission rate  
 566 estimate of  $344 \pm 130 \text{ ktons CH}_4 \text{ yr}^{-1}$ , which is about three times higher than the UNFCCC  
 567 reported national emissions from the O&G industry for Romania. Mole fraction measurements  
 568 carried out in raster flight tracks over wider areas lacked meteorological measurements and  
 569 therefore could not be used to derive direct estimates of emission rates. To support the  
 570 evaluation, simulations with two numerical atmospheric models were carried out and the  
 571 simulated CH<sub>4</sub> fields were compared with the measurements. Due to the difficult  
 572 meteorological conditions, direct quantitative evaluation remains challenging, but the  
 573 comparison of observed and simulated enhancements consistently suggests that the prior  
 574 emission rate of  $3.6 \text{ kg hr}^{-1} \text{ site}^{-1}$  used in the models is too low. In addition, the correlation of  
 575 measured and simulated CH<sub>4</sub> enhancements for the raster flights over larger areas is consistent  
 576 with the correlations observed in mass balance flights around well-defined production clusters,  
 577 indicating the validity of the derived emission factors for a large part of the southern Romanian  
 578 O&G production region. We conclude that the top-down emission estimates derived here from  
 579 airborne surveys over larger regions support the previously published emission rate estimates



580 derived from ground-based bottom-up quantifications during the ROMEO 2019 campaign.  
581 These results confirm that O&G methane emissions in 2019 were much higher than reported to  
582 UNFCCC.

583 **Data availability.** In-situ measurements and outputs of model simulations along flight tracks  
584 are available from Maazallahi et al. (2024a).

585 **Code availability.** MATLAB® codes for investigation of in-situ measurements from circular-  
586 pattern and raster flights and outputs of model simulations are available from Maazallahi et al.  
587 (2024b).

588 **Acknowledgements.** The ROMEO project was supported by the Climate and Clean Air  
589 Coalition (CCAC) Oil and Gas Methane Science Studies (MMS) hosted by the United Nations  
590 Environment Programme UNEP. Funding was provided by the Environmental Defense Fund,  
591 Oil and Gas Climate Initiative, European Commission, and CCAC. This project received  
592 further support from the H2020 Marie Skłodowska-Curie project Methane goes Mobile –  
593 Measurements and Modelling (MEMO<sup>2</sup>; <https://h2020-memo2.eu/>), grant number 722479. The  
594 modeling work used resources of the Deutsches Klimarechenzentrum (DKRZ) granted by its  
595 Scientific Steering Committee (WLA) under project ID bd0617 to perform the MECO(3)  
596 simulations.

597 **Competing interests.** At least one of the (co-) authors is a member of the editorial board of  
598 Atmospheric Chemistry and Physics. The authors have no other competing interests to declare.

599 **Author contributions.** MLS, SAC, SG, AP, and MA, carried out and evaluated airborne  
600 measurements, HM carried out the quantitative data evaluation, SJS carried out the  
601 meteorological analysis, FS supported the data analysis, MS, DB, MM, PJ, carried out the  
602 atmospheric simulations, AV, HDvdG, SD, and NVS provided inventory information, SS, MA,  
603 AC and TR designed and planned the study, HM and TR drafted the manuscript.

## 604 References

- 605 Allen, D. T., Torres, V. M., Thomas, J., Sullivan, D. W., Harrison, M., et al.: Measurements of  
606 methane emissions at natural gas production sites in the United States, Proc. Natl. Acad.  
607 Sci. U. S. A., 110, 17768-17773, 10.1073/pnas.1304880110, 2013.
- 608 Alvarez, R. A., Zavala-Araiza, D., Lyon, D. R., Allen, D. T., Barkley, Z. R., et al.: Assessment of  
609 methane emissions from the US oil and gas supply chain, Science, 361, 186-188,  
610 10.1126/science.aar7204, 2018.
- 611 Baldauf, M., Seifert, A., Förstner, J., Majewski, D., Raschendorfer, M., et al.: Operational  
612 Convective-Scale Numerical Weather Prediction with the COSMO Model: Description and  
613 Sensitivities, Monthly Weather Review, 139, 3887-3905, <https://doi.org/10.1175/MWR-D-10-05013.1>, 2011.
- 614
- 615 Brandt, A. R., Heath, G. A., Kort, E. A., O'Sullivan, F., Pétron, G., et al.: Methane Leaks from  
616 North American Natural Gas Systems, Science, 343, 733-735,  
617 doi:10.1126/science.1247045, 2014.
- 618 Brunner, D., Kuhlmann, G., Marshall, J., Clément, V., Fuhrer, O., et al.: Accounting for the  
619 vertical distribution of emissions in atmospheric CO<sub>2</sub> simulations, Atmos. Chem. Phys., 19,  
620 4541-4559, 10.5194/acp-19-4541-2019, 2019.





- 621 Collins, W. J., Webber, C. P., Cox, P. M., Huntingford, C., Lowe, J., et al.: Increased importance  
622 of methane reduction for a 1.5 degree target, *Environmental Research Letters*, 13, 054003,  
623 10.1088/1748-9326/aab89c, 2018.
- 624 Conley, S., Faloon, I., Mehrotra, S., Suard, M., Lenschow, D. H., et al.: Application of Gauss's  
625 theorem to quantify localized surface emissions from airborne measurements of wind and  
626 trace gases, *Atmos. Meas. Tech.*, 10, 3345-3358, 10.5194/amt-10-3345-2017, 2017.
- 627 Delre, A., Hensen, A., Velzeboer, I., van den Bulk, P., Edjabou, M. E., et al.: Methane and  
628 ethane emission quantifications from onshore oil and gas sites in Romania, using a tracer  
629 gas dispersion method, *Elementa: Science of the Anthropocene*, 10,  
630 10.1525/elementa.2021.000111, 2022.
- 631 Denier van der Gon, H. A. C., Kuenen, J., Boleti, E., Muntean, M., Maenhout, G., et al.:  
632 Emissions and natural fluxes Dataset, available from: [https://www.che-](https://www.che-project.eu/sites/default/files/2019-01/CHE-D2-3-V1-0.pdf)  
633 [project.eu/sites/default/files/2019-01/CHE-D2-3-V1-0.pdf](https://www.che-project.eu/sites/default/files/2019-01/CHE-D2-3-V1-0.pdf), (last access: 06 Dec. 2023),  
634 2018., 2018.
- 635 E-PRTR: European Industrial Emissions Portal. Available from:  
636 <https://industry.eea.europa.eu/explore/explore-by-pollutant>, last access 06 Dec. 2023.,  
637 2023.
- 638 EDGAR: Emissions Database for Global Atmospheric Research. Available from:  
639 <https://edgar.jrc.ec.europa.eu/>, last access: 06 Dec. 2023, 2023.
- 640 European-Commission: Deal on first-ever EU law to curb methane emissions,  
641 [https://ec.europa.eu/commission/presscorner/detail/en/IP\\_23\\_5776](https://ec.europa.eu/commission/presscorner/detail/en/IP_23_5776), 2023.
- 642 Fernandez, J. M., Maazallahi, H., France, J. L., Menoud, M., Corbu, M., et al.: Street-level  
643 methane emissions of Bucharest, Romania and the dominance of urban wastewater,  
644 *Atmospheric Environment: X*, 13, 100153, <https://doi.org/10.1016/j.aeaoa.2022.100153>,  
645 2022.
- 646 Gonzalez Moguel, R., Vogel, F., Ars, S., Schaefer, H., Turnbull, J. C., et al.: Using carbon-14 and  
647 carbon-13 measurements for source attribution of atmospheric methane in the Athabasca  
648 oil sands region, *Atmos. Chem. Phys.*, 22, 2121-2133, 10.5194/acp-22-2121-2022, 2022.
- 649 Gupta, H. V., Kling, H., Yilmaz, K. K., and Martinez, G. F.: Decomposition of the mean squared  
650 error and NSE performance criteria: Implications for improving hydrological modelling,  
651 *Journal of Hydrology*, 377, 80-91, <https://doi.org/10.1016/j.jhydrol.2009.08.003>, 2009.
- 652 Harriss, R., Alvarez, R. A., Lyon, D., Zavala-Araiza, D., Nelson, D., et al.: Using Multi-Scale  
653 Measurements to Improve Methane Emission Estimates from Oil and Gas Operations in  
654 the Barnett Shale Region, Texas, *Environmental Science & Technology*, 49, 7524-7526,  
655 10.1021/acs.est.5b02305, 2015.
- 656 Hersbach, H., Bell, B., Berrisford, P., Biavati, G., Horányi, A., et al.: ERA5 hourly data on single  
657 levels from 1940 to present, Copernicus Climate Change Service (C3S) Climate Data Store  
658 (CDS), DOI: 10.24381/cds.adbb2d47, last access 06 Dec. 2023, 2023.
- 659 IEA: Global Methane Tracker 2022, [https://www.iea.org/reports/global-methane-tracker-](https://www.iea.org/reports/global-methane-tracker-2022)  
660 [2022](https://www.iea.org/reports/global-methane-tracker-2022), last access: 2 November 2022., 2023.
- 661 Jähn, M., Kuhlmann, G., Mu, Q., Haussaire, J. M., Ochsner, D., et al.: An online emission  
662 module for atmospheric chemistry transport models: implementation in COSMO-GHG  
663 v5.6a and COSMO-ART v5.1-3.1, *Geosci. Model Dev.*, 13, 2379-2392, 10.5194/gmd-13-  
664 2379-2020, 2020.
- 665 Johnson, M. R., Tyner, D. R., Conley, S., Schwietzke, S., and Zavala-Araiza, D.: Comparisons of  
666 Airborne Measurements and Inventory Estimates of Methane Emissions in the Alberta



- 667 Upstream Oil and Gas Sector, *Environmental Science & Technology*, 51, 13008-13017,  
668 10.1021/acs.est.7b03525, 2017.
- 669 Kerkweg, A., and Jöckel, P.: The 1-way on-line coupled atmospheric chemistry model system  
670 MECO(n) – Part 1: Description of the limited-area atmospheric chemistry model  
671 COSMO/MESSy, *Geosci. Model Dev.*, 5, 87-110, 10.5194/gmd-5-87-2012, 2012.
- 672 Klausner, T., Mertens, M., Huntrieser, H., Galkowski, M., Kuhlmann, G., et al.: Urban  
673 greenhouse gas emissions from the Berlin area: A case study using airborne CO<sub>2</sub> and CH<sub>4</sub>  
674 in situ observations in summer 2018, *Elementa: Science of the Anthropocene*, 8,  
675 10.1525/elementa.411, 2020.
- 676 Knoben, W. J. M., Freer, J. E., and Woods, R. A.: Technical note: Inherent benchmark or not?  
677 Comparing Nash–Sutcliffe and Kling–Gupta efficiency scores, *Hydrol. Earth Syst. Sci.*, 23,  
678 4323-4331, 10.5194/hess-23-4323-2019, 2019.
- 679 Korbeń, P., Jagoda, P., Maazallahi, H., Kammerer, J., Nęcki, J. M., et al.: Quantification of  
680 methane emission rate from oil and gas wells in Romania using ground-based  
681 measurement techniques, *Elementa: Science of the Anthropocene*, 10,  
682 10.1525/elementa.2022.00070, 2022.
- 683 Kuenen, J., Dellaert, S., Visschedijk, A., Jalkanen, J.-P., Super, I., and Denier van der Gon, H.:  
684 CAMS-REG-v4: a state-of-the-art high-resolution European emission inventory for air  
685 quality modelling, *Earth Syst. Sci. Data*, 14, 491–515, [https://doi.org/10.5194/essd-14-491-](https://doi.org/10.5194/essd-14-491-2022)  
686 2022, 2022.
- 687 Lee, Y., and Deming, D.: Evaluation of thermal conductivity temperature corrections applied  
688 in terrestrial heat flow studies, *Journal of Geophysical Research: Solid Earth*, 103, 2447-  
689 2454, <https://doi.org/10.1029/97JB03104>, 1998.
- 690 Lopez, M., Sherwood, O. A., Dlugokencky, E. J., Kessler, R., Giroux, L., et al.: Isotopic signatures  
691 of anthropogenic CH<sub>4</sub> sources in Alberta, Canada, *Atmos. Environ.*, 164, 280-288,  
692 <https://doi.org/10.1016/j.atmosenv.2017.06.021>, 2017.
- 693 Lu, X., Harris, S. J., Fisher, R. E., France, J. L., Nisbet, E. G., et al.: Isotopic Signatures of Major  
694 Methane Sources in the Coal Seam Gas Fields and Adjacent Agricultural Districts,  
695 Queensland, Australia, *Atmos. Chem. Phys.*, 2021, 1-36, 10.5194/acp-2021-76, 2021.
- 696 Maazallahi, H., Stavropoulou, F., Sutanto, S. J., Steiner, M., Brunner, D., Mertens, M., Jöckel,  
697 P., Visschedijk, A., Denier van der Gon, H., Dellaert, S., Velandia Salinas, N., Schwietzke, S.,  
698 Zavala-Araiza, D., Ghemulet, S., Pana, A., Ardelean, M., Corbu, M., Calcan, A., Conley, S. A.,  
699 Smith, M. L., Röckmann, T.: Data for Airborne in-situ quantification of methane emissions  
700 from oil and gas production in Romania, Integrated Carbon Observation System (ICOS)  
701 [data set], [https://fileshare.icos-cp.eu/apps/files/?dir=/ROMEO\\_Flight&fileid=3286570,](https://fileshare.icos-cp.eu/apps/files/?dir=/ROMEO_Flight&fileid=3286570)  
702 2024a.
- 703 Maazallahi, H., Stavropoulou, F., Sutanto, S. J., Steiner, M., Brunner, D., Mertens, M., Jöckel,  
704 P., Visschedijk, A., Denier van der Gon, H., Dellaert, S., Velandia Salinas, N., Schwietzke, S.,  
705 Zavala-Araiza, D., Ghemulet, S., Pana, A., Ardelean, M., Corbu, M., Calcan, A., Conley, S. A.,  
706 Smith, M. L., Röckmann, T.: MATLAB® code for evaluation of airborne in-situ  
707 measurements and model simulations, Zenodo, [code],  
708 <https://doi.org/10.5281/zenodo.12701604>, 2024b.
- 709 Maazallahi, H., Fernandez, J. M., Menoud, M., Zavala-Araiza, D., Weller, Z. D., et al.: Methane  
710 mapping, emission quantification, and attribution in two European cities: Utrecht (NL) and  
711 Hamburg (DE), *Atmos. Chem. Phys.*, 20, 14717-14740, 10.5194/acp-20-14717-2020, 2020.



- 712 Menoud, M., van der Veen, C., Necki, J., Bartyzel, J., Szénási, B., et al.: Methane (CH<sub>4</sub>) sources  
713 in Krakow, Poland: insights from isotope analysis, *Atmos. Chem. Phys.*, 2021, 13167–  
714 13185, 10.5194/acp-21-13167-2021, 2021.
- 715 Menoud, M., van der Veen, C., Maazallahi, H., Hensen, A., Velzeboer, I., et al.: CH<sub>4</sub> isotopic  
716 signatures of emissions from oil and gas extraction sites in Romania, *Elementa: Science of  
717 the Anthropocene*, 10, 10.1525/elementa.2021.00092, 2022.
- 718 Mielke-Maday, I., Schwietzke, S., Yacovitch, T. I., Miller, B., Conley, S., et al.: Methane source  
719 attribution in a U.S. dry gas basin using spatial patterns of ground and airborne ethane and  
720 methane measurements, *Elementa: Science of the Anthropocene*, 7,  
721 10.1525/elementa.351, 2019.
- 722 Nash, J. E., and Sutcliffe, J. V.: River flow forecasting through conceptual models part I — A  
723 discussion of principles, *J. Hydrol.*, 10, 282-290, [https://doi.org/10.1016/0022-  
724 1694\(70\)90255-6](https://doi.org/10.1016/0022-1694(70)90255-6), 1970.
- 725 Nickl, A. L., Mertens, M., Roiger, A., Fix, A., Amediek, A., et al.: Hindcasting and forecasting of  
726 regional methane from coal mine emissions in the Upper Silesian Coal Basin using the  
727 online nested global regional chemistry–climate model MECO(n) (MESSy v2.53), *Geosci.  
728 Model Dev.*, 13, 1925-1943, 10.5194/gmd-13-1925-2020, 2020.
- 729 Nisbet, E. G., Fisher, R. E., Lowry, D., France, J. L., Allen, G., et al.: Methane Mitigation:  
730 Methods to Reduce Emissions, on the Path to the Paris Agreement, *Reviews of Geophysics*,  
731 58, 2020.
- 732 Röckmann, T., Eyer, S., van der Veen, C., Popa, M. E., Tuzson, B., et al.: In situ observations of  
733 the isotopic composition of methane at the Cabauw tall tower site, *Atmos. Chem. Phys.*,  
734 16, 10469-10487, 10.5194/acp-16-10469-2016, 2016.
- 735 Saarnio, S., Winiwarter, W., and Leitão, J.: Methane release from wetlands and watercourses  
736 in Europe, *Atmos. Environ.*, 43, 1421-1429,  
737 <https://doi.org/10.1016/j.atmosenv.2008.04.007>, 2009.
- 738 Saunio, M., Stavert, A. R., Poulter, B., Bousquet, P., Canadell, J. G., et al.: The Global Methane  
739 Budget 2000-2017, *Earth Syst Sci Data*, 12, 1561-1623, 10.5194/essd-12-1561-2020, 2020.
- 740 Shindell, D., Ravishankara, A. R., Kuylenstierna, J. C. I., Michalopoulou, E., Höglund-Isaksson,  
741 L., et al.: Global Methane Assessment: Benefits and Costs of Mitigating Methane Emissions,  
742 United Nations Environment Programme and Climate and Clean Air Coalition, Nairobi:  
743 United Nations Environment Programme., 2021.
- 744 Stavropoulou, F., Vinković, K., Kers, B., de Vries, M., van Heuven, S., et al.: High potential for  
745 CH<sub>4</sub> emission mitigation from oil infrastructure in one of EU's major production regions,  
746 *Atmos. Chem. Phys.*, 23, 10399-10412, 10.5194/acp-23-10399-2023, 2023.
- 747 Szopa, S., Naik, V., Adhikary, B., Artaxo, P., Berntsen, T., et al.: Short-lived Climate Forcers, in:  
748 *Climate Change 2021 – The Physical Science Basis: Working Group I Contribution to the  
749 Sixth Assessment Report of the Intergovernmental Panel on Climate Change*, edited by:  
750 Intergovernmental Panel on Climate, C., Cambridge University Press, Cambridge, 817-922,  
751 2021.
- 752 UNFCCC: Paris Agreement to the United Nations Framework Convention on Climate Change,  
753 T.I.A.S. No. 16-1104, 2015.
- 754 UNFCCC: Greenhouse Gas Inventory Data—Comparison by Gas.  
755 [https://di.unfccc.int/comparison\\_by\\_gas](https://di.unfccc.int/comparison_by_gas), 2023., 2023a.
- 756 UNFCCC, Romania. 2023 Common Reporting Format (CRF) Table,  
757 <https://unfccc.int/documents/627660> 2023b



758 Weller, Z. D., Hamburg, S. P., and von Fischer, J. C.: A National Estimate of Methane Leakage  
759 from Pipeline Mains in Natural Gas Local Distribution Systems, *Environmental Science &*  
760 *Technology*, 54, 8958-8967, 10.1021/acs.est.0c00437, 2020.

761 Winterstein, F., and Jöckel, P.: Methane chemistry in a nutshell – the new submodels CH4  
762 (v1.0) and TRSYNC (v1.0) in MESSy (v2.54.0), *Geosci. Model Dev.*, 14, 661-674,  
763 10.5194/gmd-14-661-2021, 2021.

764